SHOCK-INDUCED CHEMICAL REACTIONS IN NICKEL–ALUMINUM POWDER MIXTURES: RADIATION PYROMETER MEASUREMENTS

Mark B. BOSLOUGH
Sandia National Laboratories, Albuquerque, NM 87185, USA

Received 18 May 1989

Time-resolved emission of visible and near-infrared thermal radiation has been measured from powders of pure nickel and mixed nickel–aluminum shocked to peak pressures of 14 GPa. Temperatures determined from the measurements indicate that the Ni–Al mixture has a source of heat in addition to that supplied by shock compression. The extra heat, produced on a time scale of 100 ns, is inferred to come from an exothermic reaction between the two metals forming a binary alloy. If the alloy is Ni_3Al, the measured temperatures are consistent with prompt shock-induced reaction of at least 45% of the reactants.

1. Introduction

Observations of shock-induced chemical reactions in solids are numerous [1,2]. One such reaction is the subject of the present research. It was discovered by Horie et al. [3] who used explosive-loading techniques to shock nickel–aluminum powder compacts. According to analysis of the shocked material, the major end-product was ordered Ni_3Al, with a shock temperature of about 500°C required for initiation. Other products included NiAl, Ni_2Al_3, and $NiAl_3$. While such shock-recovery experiments can determine many features of shock-controlled chemical reactions, they cannot provide direct data on rates and mechanisms. To attain this information, shock-temperature experiments are required.

For highly exothermic synthesis reactions the most sensitive variable is temperature. For many such reactions there are no large volume or pressure changes that would give significant differences in pressure–volume shock states (Hugoniots). For example, Hugoniot measurements were used to demonstrate that reactions forming tin sulfide from its components can take place under shock [4], but the relative error in determining reaction completeness was as much as 30% owing to uncertainties in the measured Hugoniot and its relative insensitivity to differences between the equations of state of the reactants and products. By contrast, precise measurements of shock temperatures of reactive powders can be compared to calculated (or measured) temperatures for shocked inert powders to more accurately determine the amount of reaction. Radiation pyrometry was one of the approaches [5,6], used to measure thermal radiation from Ni–Al powders in a configuration designed to simulate earlier recovery experiments [3]. A brief emission of light consistent with the presence of temperatures as high as 5000 K was observed [6], and was taken to be evidence for shock-induced chemical reactions on a submicrosecond time scale. Similar measurements of infrared radiation emitted from shocked Al/Fe_2O_3 powders by Hornig et al. [7], led to the same conclusion. In both cases, extremely high temperatures exist only briefly, and low emissivity values are associated with them. This suggests that the shock energy in the powders is localized, resulting in temperature heterogeneities.

The present experiments were performed to isolate the early light emission from that due to a homogeneous, equilibrium temperature increase associated with shock compression and chemical reaction. The nickel–aluminum system was studied because: (1) recovery experiments have demonstrated shock-induced reactions and identified the products [3], (2) it has been theoretically modelled [8,9], (3) the large heat of reaction leads to a measurable temperature increase for partial reactions, (4) reactants and products are all metals, and therefore

0 009-2614/89/$ 03.50

graybody emitters (a requirement for radiation pyrometry) and (5) the alloys have useful applications, and are candidates for industrial shock processing.

2. Experimental

Spectral radiance of visible and near-infrared light radiated from the shocked sample is measured simultaneously at four different wavelengths with a radiation pyrometer [10]. A least-squares fit to these data determines a time-resolved temperature and effective emissivity. The target consists of a thin (about 0.5 mm) powder layer sandwiched between a copper driver and a lithium fluoride window. The thickness/diameter ratio of the powder layer is small, so the strain experienced by the center portion of the sample remains uniaxial, and the shock pulse quickly reverberates the powder up to the peak pressure (14 GPa). A mask obscures the sample edge, where rarefactions enter and disrupt the uniaxial flow. Impact of a 63 mm diameter projectile launched from a gas gun [11] generates the shock wave. Impact velocities of 1.18 km/s were employed, and the projectiles carried copper impactors. The target chamber was evacuated to eliminate air shocks, and the samples were in contact with vacuum, to minimize residual air in the pore space.

Two powders were investigated: an inert powder of 99.9% pure nickel (CERAC N-1089) with a 2 μm mean particle size, and a stoichiometric mixture (87% Ni, 13% Al by weight) of the same nickel with 99.5% pure aluminum powder (CERAC A-1183) of 1 μm mean particle size. The reactive mixture consists of only 13% aluminum by weight, so pure nickel was chosen to represent the inert powder. It has similar density, compressibility, and mechanical properties, and should therefore have a similar shock-compression response. Moreover, the similarity of spectral emissivity is important for a comparitive study based on optical measurements. The details of the two experiments are summarized in table 1.

3. Results

Spectral radiance histories are shown in figs. 1 and 2. The origins of the time axes coincide with arrival of the initial shock wave at the powder-window interface. In both cases, the radiance history consists of an initial pulse at all four wavelengths, followed

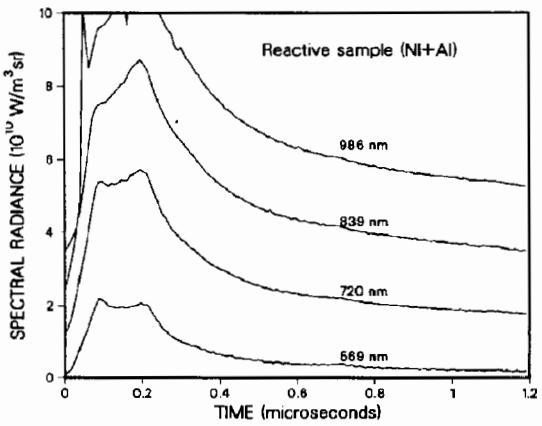

Fig. 1. Time-resolved spectral radiances for Ni–Al experiment 2208. Shock reaches powder/window interface at $t=0$. Data for each wavelength is vertically offset by 10^{10} W/m^3 sr above the next-shorter wavelength. Shortest wavelength data is not offset.

Table 1
Summary of experiments

Experiment number	Powder type	Initial density		Window material	Velocity (km/s)
		(g/cm^3)	(% of solid)		
2208	Ni–Al [a]	2.96	43	LiF	1.183
2209	Ni	3.36	38	LiF	1.184

[a] 87% Ni, 13% Al by weight.

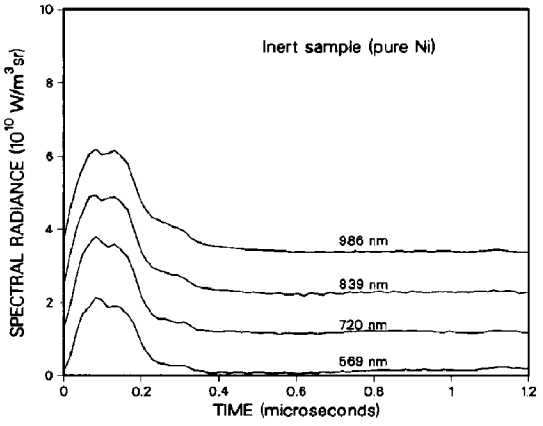

Fig. 2. Time-resolved spectral radiances for Ni experiment 2209, plotted in same manner as data in fig. 1.

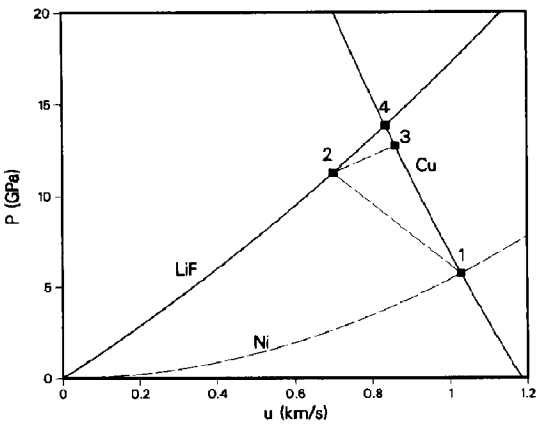

Fig. 4. Pressure-particle velocity diagram for powder experiments. Numbered states correspond to those in fig. 3.

by a decay. The initial pulses have double peaks; one corresponds to the initial shock wave, and the other is due to a twice-reflected shock that has completed one round trip through the thin sample layer, as illustrated by the x–t and P–u diagrams in figs. 3 and 4, respectively.

Ideally, the initial pulse would be sharply defined, with a nearly instantaneous rise time. However, any deviation from parallelism between the plane of the shock front and the sample-window interface will prevent simultaneous arrival. Instead, the intersection of the two planes forms a line that sweeps across the field of view. The time required to complete the sweep is proportional to the aperture diameter (19 mm), and inversely proportional to the shock velocity (less than 2 km/s). Angles between the surfaces of the powder pellets were as great as 0.001 rad, contributing further to shock wave tilt. Other factors include possible non-planarity of the shock wave due to lack of uniformity in the initial density of the powder, and non-zero rise time of the shock.

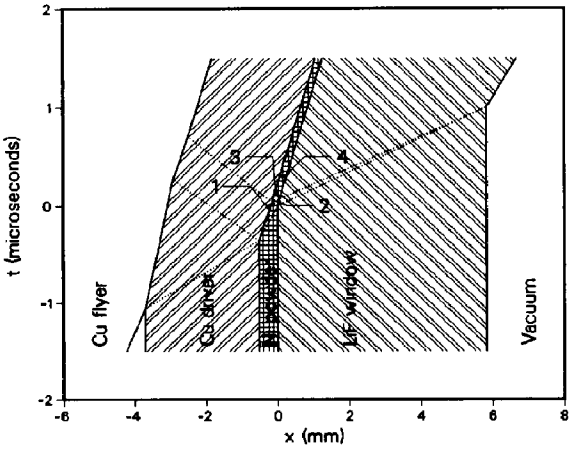

Fig. 3. Distance–time diagram for powder experiments. Shocks and rarefaction waves are represented by dotted lines. Numbers refer to states in nickel.

There are obvious differences in the data displayed in figs. 1 and 2. In addition to the greater intensities exhibited by the mixed powder, the decay rate is longer, and the spectral radiance ratios for different wavelengths are different than for the nickel. These data can be expressed in more useful terms by fitting them to the graybody distribution function,

$$N(\lambda)=\alpha\epsilon C_1\lambda^{-5}[\exp(C_2/\lambda T-1)]^{-1}, \qquad (1)$$

where α is the fraction of the area within the pyrometer field of view that is radiating light at temperature T, ϵ is the emissivity of the radiating surface, $N(\lambda)$ is the measured spectral radiance at wavelength λ, and C_1 and C_2 are known constants. Because $N(\lambda)$ is measured at four different wavelengths, there are four equations with two unknowns, and time-resolved values for ϵ and T can be determined. Since α and ϵ cannot be independently determined, their product is defined as the "effective emissivity". For uniformly heated material, 100% of the surface within the field of view is at the same temperature, and the effective emissivity is equal to

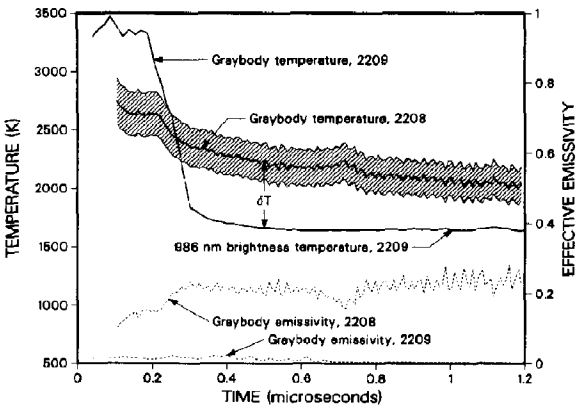

Fig. 5. Time-resolved temperature and emissivities, calculated from data in figs. 1 and 2. Numbers refer to experiments in table 1. Hatched band indicates uncertainties from least-squares fit.

the true emissivity of the surface. However, if the sample is heterogeneously heated, only some fraction of the area radiates at high temperature, and the effective emissivity is reduced from the true emissivity by the fractional area α.

The time-resolved temperature of the mixed powder is shown in fig. 5. The initial light pulse corresponds to a temperature of nearly 2800 K, with an effective emissivity of about 0.1. After approximately 500 ns, the temperature drops to about 2250 K, and the emissivity reaches a relatively stable value. This rapid cooling is consistent with heat conduction eliminating temperature heterogeneities. Any nonuniformity accompanying pore collapse and local plastic deformation is likely to have spatial variation on the same scale as the powder particle size. Temperature heterogeneities on the order of 1 μm disappear in less than 500 ns leaving a uniformly radiating surface with an effective emissivity equal to its true emissivity. The final value of 0.24 is consistent with for nickel emissivities, which vary between 0.12 and 0.37 depending on temperature and surface quality.

The time-resolved temperature for the pure nickel powder is also shown in fig. 5. It is initially higher than that of the mixed powder, presumably due to the slight differences in thermomechanical properties that lead to energy localization, and also drops rapidly in the first two or three hundred nanoseconds. Unlike the mixed powder, however, the effective emissivity starts much lower and does not increase. Pure nickel should have a slightly higher emissivity than the mixed powder; an admixture of aluminum into nickel would tend to lower the emissivity of the pellet surface (the pure pellets are darker in appearance than the mixed pellets – corresponding to higher emissivity). After 400 ns, the measured temperature begins to increase, while the emissivity drops to extremely low values. This happens when the spectral radiance from the sample drops below background levels; other experiments have shown that light can be weakly scattered from outside the direct field of view of the pyrometer (the scattering has subsequently been eliminated by a minor modification of the target design). This scattered light has a spectral radiance below about 10^9 W/m^3 sr, and is negligible unless the light radiated from the sample is just as weak. Nevertheless, an upper bound can be calculated for the bulk temperature by assuming an effective emissivity of 0.24 ($\epsilon=0.24$, $\alpha=1.0$) and using the longest wavelength (least likely to be affected by scattered radiation) to determine the brightness temperature from eq. (1). The brightness temperature assumes that all the light of a given wavelength is thermal radiation coming from a uniformly heated surface with an emissivity of 0.24. Since some fraction of the measured light is actually scattered from another source, this brightness temperature (which remains less than about 1700 K, see fig. 5), is an upper bound. The brightness temperature is not plotted for the first few hundred nanoseconds, when the temperature distribution is known to be heterogeneous.

6. Discussion

The temperature of the shocked nickel–aluminum powder mixture is about 2250 K when thermal equilibrium is reached. At the equivalent time in the pure nickel sample, an experimental upper bound for the temperature is about 1650 K. The shock temperature of the mixed powder is thus at least $\delta T=600$ K higher than that of the nickel powder. For low density, porous metals, the snowplow model (a special case of the P–α model [12]) is used to estimate equilibrium shock temperatures. It assumes that the first shock wave increases the initial density of the powder (ρ_{00}), to its full density (ρ_0). Reflected shocks increase the pressure of the crushed-up pow-

der, but increase the density by only a negligible amount. The Hugoniot of the powder for the first shock is given simply by

$$P = u^2 \rho_0 \rho_{00} / (\rho_0 - \rho_{00}) , \quad (2)$$

where P is the shock pressure and u is the particle velocity. The porous Hugoniot of nickel powder is plotted in fig. 4. Impedance matching this Hugoniot to the inverted Hugoniot for copper centered on the impact velocity of 1.18 km/s gives an initial shock pressure of about 6 GPa. The net increase in internal energy is given by the Rankine–Hugoniot equation

$$\Delta E = \tfrac{1}{2} P (1/\rho_{00} - 1/\rho_0) , \quad (3)$$

and the increase in temperature is approximated by $\Delta T = \Delta E / C_p$ where $C_p = 520$ J/gK is used to approximate the specific heat of the nickel. In the snowplow model, no further energy is acquired by the nickel in reverberating to the peak pressure of 14 GPa. In reality, there is a small volume change after the initial shock, but it is so small compared to the volume change on crushing that it can be ignored. The estimated temperature increase is about 1100 K, and when added to the initial temperature gives a calculated shock temperature of about 1400 K, somewhat less than the experimental upper bound. If the crush strength of the powder is significant, the snowplow assumptions are no longer valid, and the actual temperature would be lower.

The shock component of temperature increase will be somewhat less for the mixed powder, because of slightly different thermomechanical properties. According to ref. [13], the energy released by the reaction $3Ni + Al \rightarrow Ni_3Al$ is about 40 kJ/mol of Ni_3Al at standard conditions, which is sufficient to raise the adiabatic temperature by about 1300 K. The measured temperature difference of at least 600 K is, therefore, equivalent to prompt shock-induced reaction of at least 45% of the material.

5. Conclusions

Radiation pyrometry measurements have been used to demonstrate the existence, time scale and completeness of prompt shock-induced chemical reactions in the Ni–Al system. By varying the shock pressure and porosity of starting materials, such experiments can determine the conditions required for shock initiation of these reactions. Other highly reactive solids are candidates for shock-temperature measurements to determine the thresholds, rates and energetics of their reactions under shock, with time resolution limited by the equilibration time for temperature heterogeneities in powders. With these measurements, the underlying mechanisms controlling shock-induced chemical reactions in solids can be studied.

Acknowledgement

This work was performed at Sandia National Laboratories supported by the US Department of Energy under contract #DE-AC04-76DP00789. M.U. Anderson, M.R. Lewis and D.E. Wackerbarth provided expert technical assistance.

References

[1] G.A. Adadurov, V.I. Gol'danskii and P.A. Yampolskii, Mendeleev Chem. J. 18 (1973) 92.
[2] R.A. Graham, in: Shock waves in condensed matter 1987, eds. S.C. Schmidt and N.C. Holmes (North-Holland, Amsterdam, 1988) p. 11.
[3] Y. Horie, R.A. Graham and I.K. Simonsen, Mater. Letters 3 (1985)354.
[4] S.S. Batsanov, G.S. Doronin, S.V. Klochkov and A.I. Teut, Combust. Explos. Shock Waves 22 (1986) 134.
[5] M.B. Boslough and R.A. Graham, Chem. Phys. Letters 121 (1985) 446.
[6] M.B. Boslough, R.A. Graham and D.M. Webb, in: Shock waves in condensed matter, ed. Y.M. Gupta (Plenum Press, New York, 1986) p. 755.
[7] H.C. Hornig, J.W. Kury, R.L. Simpson, F.H. Helm and W.G. Von Holle, Proceedings of the Eleventh International Pyrotechnics Seminar (IIT Research Institute, Chicago, 1986) p. 699.
[8] Y. Horie and M.E. Kipp, J. Appl. Phys. 63 (1988) 5718.
[9] P.A. Taylor, M.B. Boslough and Y. Horie, in: Shock waves in condensed matter 1987, eds. S.C. Schmidt and N.C. Holmes (North-Holland, Amsterdam, 1988) p. 395.
[10] M.B. Boslough and T.J. Ahrens, Rev. Sci. Instr. submitted for publication (1989).
[11] R.E. Setchell, in: Shock waves in condensed matter 1981, eds. W.J. Nellis, L. Seaman and R.A. Graham (AIP, New York, 1982) p. 657.
[12] W. Herrmann, J. Appl. Phys. 40 (1969) 2490.
[13] P.D. Desai, J. Phys. Chem. Ref. Data 16 (1987) p. 109.